

RADIO-SELECTED QUASARS IN THE SLOAN DIGITAL SKY SURVEY

IAN D. MCGREER¹, DAVID J. HELFAND¹, RICHARD L. WHITE²

Draft version April 11, 2021

ABSTRACT

We have conducted a pilot survey for $z > 3.5$ quasars by combining the FIRST radio survey with the SDSS. While SDSS already targets FIRST sources for spectroscopy as quasar candidates, our survey includes fainter quasars and greatly improves the discovery rate by using strict astrometric criteria for matching the radio and optical positions. Our method allows for selection of high-redshift quasars with less color bias than with optical selection, as using radio selection essentially eliminates stellar contamination. We report the results of spectroscopy for 45 candidates, including 29 quasars in the range $0.37 < z < 5.2$, with 7 having redshifts $z > 3.5$. We compare quasars selected using radio and optical criteria, and find that radio-selected quasars have a much higher fraction of moderately-reddened objects. We derive a radio-loud quasar luminosity function at $3.5 < z < 4.0$, and find that it is in good agreement with expectations from prior SDSS results.

Subject headings: quasars: general

1. INTRODUCTION

The first quasars were discovered in radio surveys once it became possible to confidently associate radio sources with optical counterparts that had unusual colors (Schmidt 1963). Subsequently it was found that quasars could be readily identified on the basis of their optical emission alone (Sandage 1965), as their roughly power-law spectral energy distributions were easily distinguishable from stellar black-body emission. Optical surveys have since dominated quasar discoveries, while the minority radio population has been used to find highly reddened quasars (Webster et al. 1995; Gregg et al. 2002; White et al. 2003; Glikman et al. 2004, 2007; Urrutia et al. 2008) and scarce, high-redshift quasars (Hook et al. 1995, 1998; Snellen et al. 2001; Benn et al. 2002; Holt et al. 2004; Carballo et al. 2006, 2008; McGreer et al. 2006). In both cases the use of radio data enables searches in regions of color space which are problematic for optical selection alone.

The Sloan Digital Sky Survey (SDSS, York et al. 2000) has assembled the largest collection of quasars to date; the DR5 catalog includes nearly 80,000 quasars found over 8000 deg² (Schneider et al. 2007). Before SDSS, only ~ 200 quasars were known at $z > 4$, and none at $z > 5$. By targeting roughly 10^5 objects for spectroscopic follow-up as candidate quasars, the SDSS has been able to uncover even the rarest sources, including ~ 60 luminous quasars at $z > 5$.

Historically, low-redshift quasars were often identified by their ultraviolet-excess relative to stars, and were thus selected from somewhat restricted regions of color space. One of the great advances of the SDSS was to select essentially all objects with stellar morphologies but non-stellar colors as quasar targets, allowing for a variety of quasars to be discovered over a wide range of redshifts, including objects with highly unusual colors (e.g.,

BALQSOs, Hall et al. 2002). However, quasar colors are not always different from those of stars. This is especially problematic at high redshift ($z > 2$), where quasar colors blend with the stellar distribution. Whether or not a given quasar is selected by the SDSS depends on its flux, redshift and intrinsic color; thus the selection function can be somewhat difficult to characterize, even if target determination is rather simple.

The sheer yield of quasars from the SDSS demonstrates that the targeting algorithms are highly effective. The completeness of the SDSS quasar survey has been studied in detail by Vanden Berk et al. (2005) and Richards et al. (2006, hereafter R06). The former obtained spectra of $\sim 20,000$ stellar objects from 278 deg² of SDSS imaging data and found that only 10 were quasars missed by SDSS targeting. The latter used simulated quasar photometry, assuming a Gaussian distribution of power-law quasar spectral energy distributions (SEDs) centered on a typical spectral index of $\alpha_\nu = -0.5$ ($F_\nu \propto \nu^{\alpha_\nu}$), to estimate the completeness of the observed quasar distribution with respect to color, luminosity, and redshift. Both studies were most effective at low redshift ($z < 2.5$) due to the relative scarcity of more distant quasars.

The SDSS also considers stellar counterparts to radio sources from the Faint Images of the Radio Sky at Twenty-Centimeters survey (FIRST, Becker et al. 1995) as primary targets. Radio selection of quasar candidates is limited in the sense that radio-bright quasars constitute only $\sim 10\%$ of the total population, and objects selected by radio emission may not be representative of the population as a whole. On the other hand, radio selection avoids many of the problems inherent in color selection, as stars do not contribute significantly to the mJy radio population and are thus easily eliminated from radio samples without regard to color. In this way, radio selection can be used to test the completeness of optical selection.

The apparent connection between black hole growth and galaxy evolution (e.g., Ferrarese & Merritt 2000) underscores the need to understand the evolution of the

Electronic address: mcgreer@astro.columbia.edu

¹ Dept. of Astronomy, Columbia University, Pupin Physics Laboratories, New York, NY 10027

² Space Telescope Science Institute, Baltimore, MD 21218

quasar population over cosmic time. Evolutionary trends in the quasar population are often characterized through luminosity functions, which require a well-understood selection function. The comoving number density of quasars has long been known to evolve strongly with redshift, peaking at $z \sim 2.5$ and declining rapidly at higher redshifts. A sample of $z > 2.75$ quasars from the Palomar Transit Grism Survey (Schmidt et al. 1995) yielded a flatter slope for the high- z quasar luminosity function than that derived for low-redshift quasars. The much larger sample of color-selected quasars from the SDSS showed a similar change in the bright-end slope, suggesting an evolution not just in the number density but also the luminosity distribution of high-redshift quasars (Fan et al. 2001; Richards et al. 2006). However, there are relatively few probes of the luminous high- z quasar population available for comparison.

In this work we examine the completeness of SDSS quasar selection at $z > 3.5$ by identifying quasar candidates drawn from the combined FIRST and SDSS data. We define a sample of high- z quasar candidates through a simple color cut which selects red SDSS counterparts to FIRST sources. This allows us to explore a wide swath of color space with minimal bias in the optical colors of high-redshift quasars. We achieve a relatively high efficiency of discovery by requiring small offsets between the radio and optical positions, practically eliminating stars from our sample. Our observations fill in gaps in the SDSS quasar selection by targeting fainter counterparts to radio sources.

We begin by summarizing the methods for targeting quasar candidates adopted by the SDSS. We describe our selection criteria in § 3 and compare the efficiencies of various selection methods. In § 4 we present spectroscopy for 45 of our candidates, including many new quasars. We place our sample in a broader context in § 5 by including results from other surveys, following which we discuss a population of moderately-reddened quasars at low redshift found primarily through radio selection, and calculate a luminosity function for radio-loud quasars at $3.5 < z < 4.0$. Finally, we present some brief conclusions and prospects for future surveys. We adopt a standard cosmology of $H_0 = 70$ km/s/Mpc, $\Omega_m = 0.3$, $\Omega_\Lambda = 0.7$.

2. SDSS QUASAR SELECTION

As our quasar sample is drawn from the SDSS, we provide a brief review of the algorithms used by SDSS to target quasars for spectroscopy before discussing our method for selecting high-redshift quasars. For a complete description of SDSS quasar selection, see Richards et al. (2002).

The SDSS has two primary criteria for targeting quasars. The first is color selection, with separate criteria for low- and high-redshift targets. The algorithm used to target quasars at $z > 2.5$ is referred to as QSO_TARGET_HIZ. Briefly, stellar sources with $15.0 < i < 20.2$ are targeted when they are far from the stellar locus in *griz* color space, or if they are within inclusion regions (and outside exclusion regions) used to target quasars at specific redshifts. This leads to a strongly redshift-dependent completeness at high redshift, as quasar colors move in and out of the stellar locus (R06). For brevity, we will refer to the QSO_TARGET_HIZ algorithm as QSO_HIZ.

The second criterion is based on matching stellar SDSS sources to FIRST radio sources; all sources having $15.0 < i < 19.1$ and a FIRST match within $2''$ are selected for spectroscopic follow-up. Targets selected in this manner have the flag QSO_FIRST³. FIRST selection allows quasar candidates that fall within the stellar locus or are otherwise missed by color selection to be targeted. However, the brighter magnitude limit adopted for QSO_FIRST selection means that few high- z quasars are identified outside of the QSO_HIZ algorithm – only $\sim 20\%$ of $z > 3$ quasars in DR5QSO have $i < 19.1$, and only 1 in 10 were targeted outside of QSO_HIZ.

Objects from the SDSS photometric database are rejected as quasar candidates if they have the fatal errors BRIGHT, SATURATED, EDGE, or BLENDED. The first three flags occur for bright objects, bleed trails of bright stars, and objects near the edge of imaging frames. The deblending algorithm separates BLENDED sources into one or more children, each of which is assigned the CHILD flag and is considered by the quasar targeting algorithm. A primary object with the BLENDED flag indicates that the attempt to deblend was unsuccessful, and thus the object’s photometry is unreliable.

3. RADIO SAMPLE SELECTION

Our survey is designed to identify $z > 3.5$ radio-loud quasars efficiently with a high level of completeness and minimal bias in optical color. Stars are the principal contaminant in optical quasar surveys and must be eliminated to achieve high efficiency. As noted in §2, SDSS uses a $2''$ radius to match with FIRST. This results in a high degree of completeness with respect to radio-optical associations, as very few radio quasars have offsets between the optical and radio positions greater than this value. In fact, due to the excellent astrometry of the two surveys, the peak of the optical/radio offsets occurs at about $0.2''$ (Schneider et al. 2007, Figure 9a). On the other hand, the number of stars in the SDSS is so large that using a $2''$ radius to identify radio quasar candidates results in significant stellar contamination. Of the quasar candidates targeted by SDSS using FIRST-only criteria (i.e., having the QSO_FIRST target flag set but no optical selection flags), only 40% are quasars, while over half are stars. This is not due to a large population of stars with mJy radio emission; rather, the stars are clearly offset from the radio positions with a distribution consistent with chance coincidence. Recent work with the SDSS has shown that the number of radio-emitting stars detected by FIRST at faint optical magnitudes is exceedingly small (Kimball et al. 2009).

Sub-arcsecond matching of FIRST and SDSS sources greatly increases the yield of quasars relative to stars, but does introduce bias against sources near the FIRST detection limit, where the astrometric uncertainties are greater. In addition, for quasars with extended radio counterparts, the fitted radio centroid may not correspond directly to the optical position. We find that using a $0.5''$ matching radius is $\gtrsim 70\%$ complete to quasars with $S_{1.4} > 2$ mJy; this will be discussed in more detail in §6.3.

³ Within the SDSS imaging database, the flags QSO_FIRST_CAP and QSO_FIRST_SKIRT are used for FIRST-selected quasar targets; however, no distinction is made between these flags and we refer to them collectively as QSO_FIRST.

TABLE 1
COMPARISON OF SELECTION METHODS

Selection	FIRST (")	Number	Quasars $z < 3.5$	Quasars $z > 3.5$	Stars	Galaxies	Unknown
QSO_HIZ	-	60237	17981 (29.9)	2859 (4.7)	30816 (51.2)	4371 (7.3)	4210 (7.0)
QSO_HIZ + red <i>ugr</i>	-	37828	1731 (4.6)	2850 (7.5)	25471 (67.3)	4028 (10.6)	3748 (9.9)
QSO_FIRST	2.0	5338	4137 (77.5)	53 (1.0)	782 (14.6)	125 (2.3)	241 (4.5)
FIRST + red <i>ugr</i>	2.0	1396	418 (29.9)	131 (9.4)	654 (46.8)	81 (5.8)	112 (8.0)
	0.5	601	313 (52.1)	112 (18.6)	56 (9.3)	40 (6.7)	80 (13.3)

NOTE. — Summary of methods used to identify quasar candidates in the SDSS. Values in each row are extracted from queries to the DR6 SpecObj table. The second column gives the FIRST matching radius for radio selection methods, and the third column gives the number of objects resulting from the query. These objects are subdivided into types using classifications from the SDSS spectro1d pipeline, with percentages of the total for each row given in parenthesis. Visual examination of the spectra will change these results at the few percent level (e.g., Schneider et al. 2007), but the numbers are representative. Note that QSO_FIRST has a limit of $r < 19.1$, while all other methods have a limit of $i < 20.2$.

The strict matching described above allows us to eliminate stars without resorting to color selection techniques, freeing us to select quasars independently of their optical properties. However, if we blindly selected optical counterparts to radio sources, we would be overwhelmed by low- z quasars. To reach the desired population at $z > 3.5$, we take advantage of Lyman- α forest absorption, which reddens all high- z quasars irrespective of their intrinsic spectral energy distribution. In particular, we expect the ultraviolet to blue wavelength range (the u and g bands in SDSS) to be strongly absorbed for $z > 3.5$ quasars, and thus colors in these bands can be used to reduce low- z quasar contamination without introducing much bias at high redshift. A thorough discussion of the changes in quasar colors with redshift in the SDSS photometric system can be found in Richards et al. (2001). In that work it is noted that at $z > 2.6$, little or no flux is expected in the u -band, while at $z > 3.5$, the $g - r$ color reddens as the Ly α forest is in the g -band.

We base our selection on the combination of a red *ugr* color cut with sub-arcsecond matching of radio and optical positions. In order to expand on SDSS selection, we target objects below the flux limit of QSO_FIRST selection. The sample is drawn from the SDSS DR6 photometric database Best.PhotoObjAll, joining the First table to obtain objects with 2'' matches to FIRST sources, and applying these criteria:⁴

1. primary survey object with stellar morphology, $15.0 < i < 20.2$
2. FIRST counterpart within 0.5''
3. $u > 20.5$ or $u - g > 1.5$
4. $g > 21.0$ or $g - r > 0.5$

The resulting sample contains 1556 objects. We then reject objects with the fatal photometric errors BRIGHT, SATURATED, and EDGE, as well as those not having the flag OK_SCANLINE set (Richards et al. 2002). This reduces the sample to 1536 candidate quasars. Of the 2484 quasars in DR5QSO with $z > 3.5$, only two do not

meet our selection criteria (ignoring the FIRST match requirement). Both are luminous ($M_i < -28$) quasars at $z \sim 3.7$, and are missed because they are unusually bright in the u band ($u \sim 20.4$ and $u - g < 1.3$). Thus we expect that our color criteria are highly complete for $z > 3.5$ quasars.

We chose to keep BLENDED objects after noticing that some of the previously identified $z > 3.5$ quasars in our sample were flagged BLENDED. Visual examination of the 76 BLENDED objects in our candidate sample showed that nearly all of them are isolated objects.

All FIRST counterparts to SDSS objects meeting the selection criteria are included, thus the radio flux limit is that of the FIRST survey, $F_{20\text{cm}} \gtrsim 1$ mJy. In some later analysis the sample will be limited to a subset of brighter radio sources with $F_{20\text{cm}} > 2$ mJy.

Table 1 compares the efficiencies of the various quasar targeting methods described in this section, based on queries to the DR6 SpecObj table. Note that the numbers shown are based on the output from the automated classification pipeline used by the SDSS, and should only be considered qualitative, as visual examination of the spectra will change the classifications at the level of a few percent. The largest sample is QSO_HIZ – over 20,000 quasars have been identified by this algorithm, with ~ 2900 at $z > 3.5$ (including DR6 results). Yet the majority of QSO_HIZ objects are stars, and only $\sim 5\%$ are $z > 3.5$ quasars. This algorithm is designed for quasars at $z > 2.5$, thus for better comparison to our sample we apply our red *ugr* color criteria and query the database for QSO_HIZ objects matching those criteria. As expected, the fraction of $z > 3.5$ quasars in the sample increases to $\sim 8\%$ and many low- z quasars are eliminated. However, the fraction of stars increases to more than two-thirds.

Radio selection using 2'' matches to FIRST sources increases the overall yield of quasars to nearly 80% and reduces the stellar contamination to $\sim 15\%$, but finds mostly low- z quasars due to the relative scarcity of the high-redshift population (especially at the brighter limit of $i < 19.1$). Imposing our red *ugr* color cut results in large numbers of both stars and quasars, but with $z > 3.5$ quasars being much more rare, stars make up nearly half of the sample when a 2'' match radius is used. Further imposing a stricter matching radius of 0.5'' reduces the

⁴ All SDSS magnitudes quoted in this work are Galactic extinction-corrected PSF magnitudes.

TABLE 2
SPECTROSCOPIC OBSERVATIONS

RA (J2000)	Dec (J2000)	r (AB)	i (AB)	$S_{1.4}$ (mJy)	$\log R^1$	ID	z	flags ²	notes
07 41 54.72	+25 20 29.6	20.49	18.45	2.97	1.32	QSO	5.194	fhg	
11 34 18.11	+28 47 13.0	18.50	18.28	3.10	1.35	QSO	3.530	f	
12 35 44.84	+32 19 45.9	18.61	18.66	1.41	1.09	QSO	3.880	b	
14 35 48.56	+20 13 21.2	18.59	18.37	7.52	1.69	QSO	0.368	b	
15 28 30.49	+32 10 43.7	18.70	17.64	3.22		QSO?		b	$z = 1.71$ from Mg II,C IV
15 52 37.42	+61 36 44.3	18.89	18.27	2.22	1.16	QSO	0.678	f	
16 05 58.85	+47 43 00.1	18.59	18.20	14.01		Star		f	
16 52 38.45	+44 28 47.9	18.27	17.68	4.29	1.18	QSO	1.080	b	
16 57 58.34	+31 14 59.8	18.49	18.15	0.71	0.81	QSO	0.384	f	
11 32 32.68	+09 14 28.1	20.10	19.44	39.90	2.85	QSO	1.576		
11 40 32.29	+24 01 18.0	20.10	19.31	3.69					
12 04 07.83	+48 45 48.2	19.97	19.53	2.64					
12 31 28.23	+18 47 14.4	19.41	19.34	11.17	2.26	QSO	3.318	h	
12 35 47.98	+09 08 01.1	20.21	19.42	2.79					
13 01 00.89	+32 07 27.5	20.17	19.30	0.74	1.23	QSO	0.510		
13 19 01.75	+11 41 38.5	20.04	19.31	2.80	1.64	QSO	0.454		
13 22 46.59	+35 28 48.5	20.12	19.50	2.80		QSO?			$z = 0.61$ from H β , [O III]
13 36 30.29	+41 19 55.6	19.85	19.31	8.84					
14 04 59.93	+18 23 46.2	20.37	19.40	1.35				h	
14 06 35.67	+62 25 43.3	19.72	19.49	11.50	2.33	QSO	3.890	h	
14 11 23.07	+08 00 42.4	20.02	19.40	1.96					
14 12 41.04	+37 01 00.9	19.92	19.66	16.42	2.55	QSO	3.368		
14 18 21.30	+42 50 20.2	20.04	19.48	214.27	3.59	QSO	3.458		
14 21 32.18	+12 57 35.9	19.45	19.49	5.99	2.09	QSO	3.831		
14 23 32.00	+05 55 04.8	20.68	19.47	2.77		Star			
14 26 34.86	+54 36 22.8	21.46	19.84	4.36	2.05	QSO	4.848	g	
14 30 53.22	+54 35 38.7	19.98	19.59	4.35	1.98	QSO	2.530		
15 34 15.26	+26 18 59.6	20.20	19.41	10.65	2.26	QSO	0.913	h	
15 35 38.50	+19 44 21.2	19.76	19.57	13.47				b	
15 40 43.73	+49 23 23.7	20.57	19.50	33.46	2.80	Galaxy	0.697		
15 42 48.90	+24 13 28.5	20.36	19.48	4.17					
16 09 53.40	+57 05 00.3	20.22	19.58	2.52	1.71	QSO	0.758		
16 21 11.07	+14 06 02.4	19.90	19.46	28.49	2.71	QSO	1.248		
16 37 05.13	+48 36 01.8	21.55	20.12	1.57	1.84	Galaxy	0.099	g	
16 37 08.30	+09 14 24.6	19.56	19.54	9.43	2.26	QSO	3.750	h	
16 50 37.63	+21 22 08.5	20.09	19.45	7.48	2.13	QSO	3.023		BAL
16 52 14.00	+44 35 30.7	19.93	19.33	2.94	1.73	QSO	2.507	h	
17 02 21.33	+46 11 13.1	19.46	19.10	1.17	1.18	QSO	1.098		
17 02 41.20	+47 37 16.9	20.42	19.60	1.56					
17 02 53.55	+23 57 58.1	19.74	19.35	19.24		Star			
17 04 12.69	+30 09 31.6	20.27	19.49	6.09	2.08	QSO	3.015		BAL
17 06 32.53	+27 58 18.5	20.85	19.81	1.70	1.64	QSO	0.493		
17 10 01.18	+38 49 09.9	19.48	19.34	2.97	1.68	QSO	3.208		
17 14 15.78	+25 58 11.6	19.83	19.28	2.78	1.63	QSO	3.170		BAL
17 20 02.17	+24 55 48.8	19.82	19.39	12.90	2.34	QSO	3.350		BAL

NOTE. — Objects with $i < 19.1$ are shown in the upper part of the table. Objects with no identifiable features are given blank entries.

¹ Radio loudness, $R = F(5 \text{ GHz})/F(2500\text{\AA})$ (see §6)

² b - BLENDED, f - QSO_FIRST target, g - g -band dropout, h - QSO_HIZ target

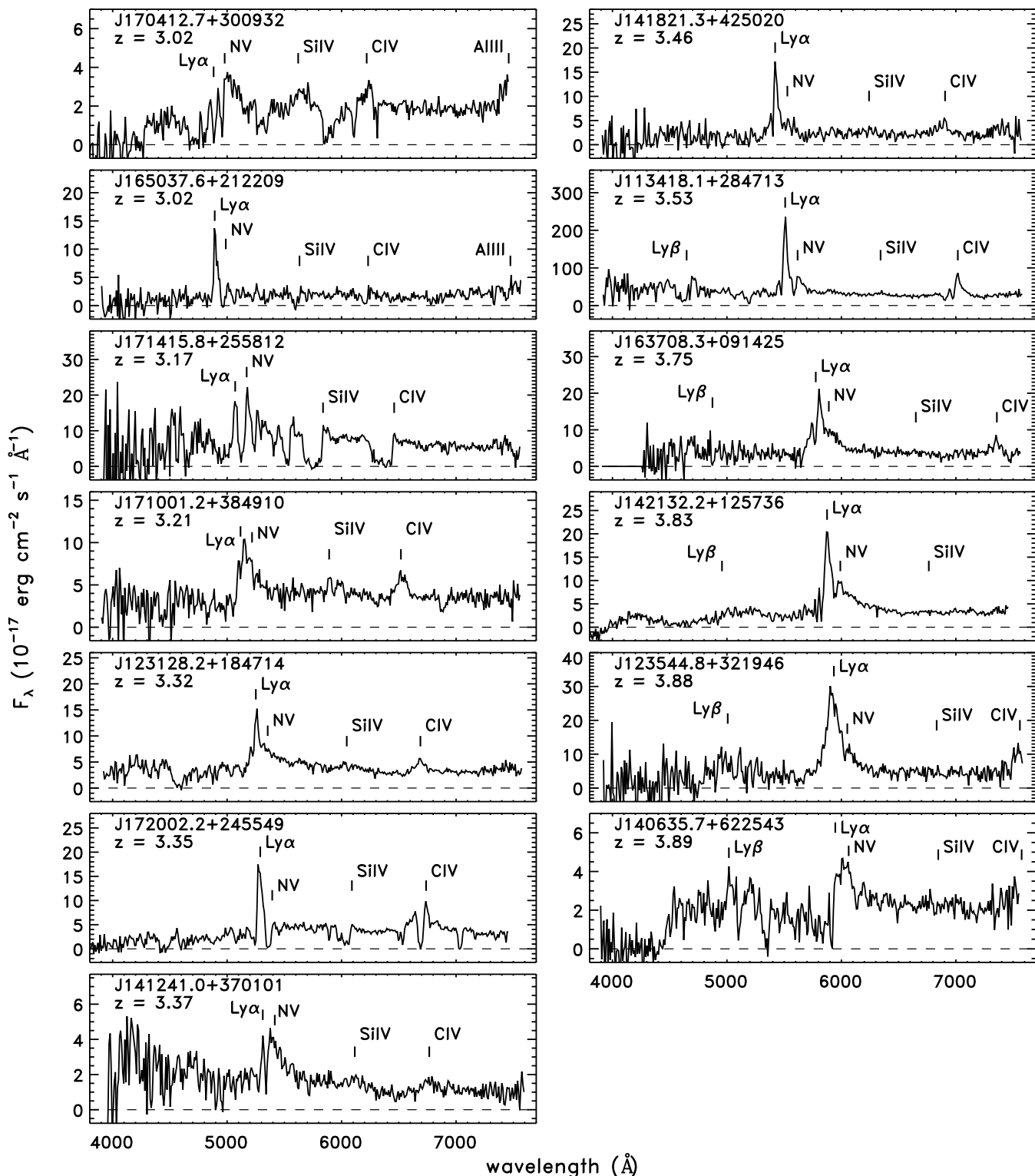


FIG. 1.— Spectra of quasars with $3 < z < 4$. Most of the $z < 3.5$ are considerably redder than SDSS quasars in the same redshift range, and several show strong BAL features. The spectra are binned to a dispersion of 10\AA for display purposes. Observed wavelengths of common emission lines are marked.

number of stars by more than a factor of 10 while losing only a handful of quasars. The final result is that over 70% of our FIRST-selected sample with red ugr colors consists of quasars, with nearly 20% at $z > 3.5$.

4. OBSERVATIONS

We constructed a sample of candidates meeting the selection criteria of the preceding section and without preexisting spectra (as of the SDSS DR6 release), and obtained low-resolution optical spectra for a total of 45 of these candidates with the 2.4m Hiltner telescope at MDM Observatory. Objects were selected for observation that were below the threshold of QSO_FIRST targeting in SDSS ($i = 19.1$), favoring sources with $i \sim 19.5$. During occasional periods of poor seeing, objects with $i < 19.1$ were observed. This included 5 objects that were flagged QSO_FIRST but for which spectra were not obtained in the SDSS. Also included in the bright sample were 4 BLENDED objects that were rejected as quasar targets by the SDSS (see §3). Finally, while most of the observed sources were u -band dropouts, three g -band dropouts were also observed.

Low-resolution spectra were obtained with the Boller & Chivens CCD Spectrograph (CCDS), equipped with a 150 grooves mm^{-1} grating centered at $\sim 5700\text{\AA}$. Nearly all of the spectra were obtained from 2008 June 2 to June 9, with one spectrum obtained on 2009 Jan 29. Nights were generally non-photometric with seeing between $1.0''$ and $1.8''$, and the slit width was set to either $1.0''$ or $1.5''$ to match the seeing. The wavelength coverage was $3900\text{--}7600\text{\AA}$ with a spectral resolution of 8.2\AA for the $1''$ slit and 12.4\AA for the $1.5''$ slit. Individual exposures were typically 900s, with total exposure times of 30-60m. Targets were observed at low airmass ($\text{secz} < 1.3$) with the slit at a PA = 0° .

The spectra were reduced using standard IRAF⁵ routines called from scripts written in Pyraf.⁶ The standard stars HZ44 and BD+284211 were observed each night for flux calibration. Wavelength calibration was provided by Xe and Ar lamps at the beginning and end of each night, though the dispersion was checked (and sometimes corrected) using night sky lines. Cosmic rays were detected in individual images using the L.A. Cosmic routines⁷ (van Dokkum 2001), and then masked when the images were combined.

Table 2 provides a catalog of the 45 candidates for which spectra were obtained at MDM. For nine objects, the spectra did not show any identifiable features, but nonzero flux was detected across the full wavelength range sampled and these objects are ruled out as $z > 3.5$ quasars based on the lack of a Ly α break. Some of these objects may be quasars at lower redshifts that did not present strong emission lines within the wavelength range covered by the MDM spectra. Two objects presented broad lines without clear identifications, and are classified as probable quasars based on the most likely interpretation for the lines. Finally, 34 of the observed

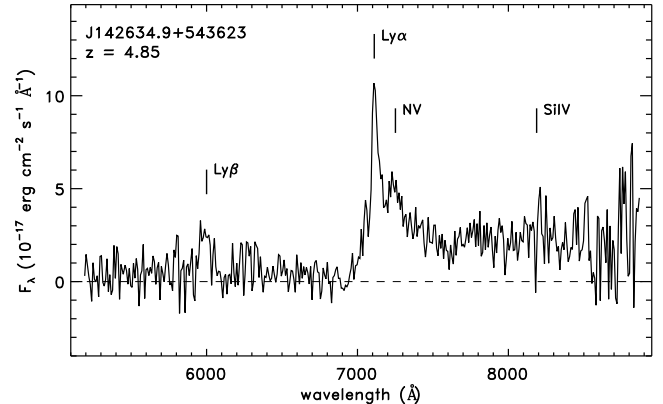


FIG. 2.— Spectrum of J142634.8+543622, with $z = 4.85$. The spectrum is binned to a dispersion of 10\AA .

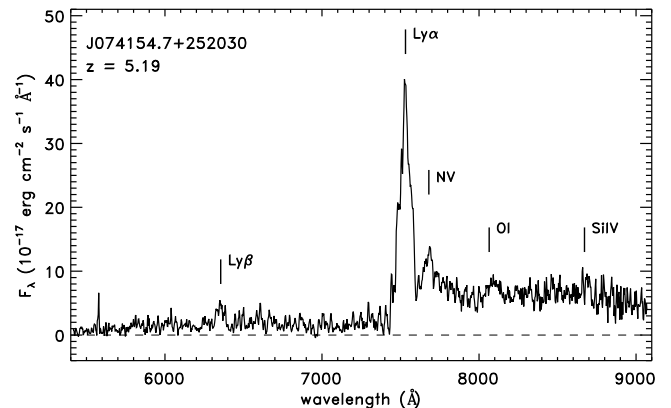


FIG. 3.— Spectrum of J074154.7+252029, with $z = 5.19$. This spectrum is unbinned, with a dispersion of 3\AA . The feature at 5577\AA is due to incomplete subtraction of the O I sky line.

candidates have identifiable features and have been assigned redshifts. This includes 3 stars (7%), 2 galaxies (4%), and 29 quasars (64%). Of the 4 BLENDED objects, at least 3 are quasars, including the fourth highest redshift overall. The three g -band dropouts yielded the lowest and highest redshifts. One is a faint galaxy at $z = 0.099$, and the other two are quasars at $z = 4.8$ and $z = 5.2$ (Figures 2 and 3). A total of 15 of the observed candidates had redshifts $z > 3$, including 7 with $z > 3.5$ (Figures 1, 2, and 3).

While none of the candidates observed at MDM had published spectra at the time they were observed, several of them have since appeared in Carballo et al. (2008). In that work, neural networks were employed on combined data from FIRST and SDSS to select quasar candidates at $z > 3.6$; not surprisingly, many of their candidates are in common with ours, including six objects observed at MDM. Of these, three are $z > 3$ quasars for which our identifications are in good agreement with theirs (J123128.2+184714, J140635.6+622543, and J172002.1+245548). The other three do not have identifications in Carballo et al. (2008), and include one object also unidentified by us (J120407.8+484548), one star (J170253.5+235758, based on Mg I and Na I absorption), and one quasar at $z = 3.32$ (J123128.2+184714).

⁵ IRAF is distributed by the National Optical Astronomy Observatories, which are operated by the Association of Universities for Research in Astronomy, Inc., under cooperative agreement with the National Science Foundation.

⁶ Pyraf is a product of the Space Telescope Science Institute, which is operated by AURA for NASA.

⁷ <http://www.astro.yale.edu/dokkum/lacosmic/>

4.1. Notes on individual sources

1. FIRST J163705.1+483601 ($z = 0.099$): One of the three g -band dropouts observed at MDM. Identification is based on narrow $H\alpha$ and $[O\ II]$ lines. The emission line strengths and radio luminosity are consistent with a mixture of star formation and AGN activity.

2. FIRST J142634.8+543622 ($z = 4.848$): Another g -dropout and the second most distant source in the sample (Figure 2). This quasar was first identified with a 900s spectrum on 2008 June 6, and on 2008 June 8 a 3600s spectrum was obtained with the grating centered at 7000\AA in order to capture more of the emission redward of $Ly\alpha$. It is not a primary quasar target in the SDSS.

3. FIRST J074154.7+252029 ($z = 5.194$): A g -dropout, but bright enough ($i = 18.5$) to be a QSO_FIRST target, though no spectrum was obtained in the SDSS. It is also a QSO_HIZ target. This object was observed with CCDS at MDM on 2009 Jan 29 with a $1''$ slit, a wavelength range of $5400\text{--}9100\text{\AA}$, and a total exposure time of 4800s. It is brighter than any $z > 5$ quasar in DR5QSO, with a derived luminosity of $M_i = -29$. Two 60s exposures were obtained in the i band with the Retrocam imager (Morgan et al. 2005) on the MDM 2.4m. The seeing was $1.2''$. The images were combined with standard IRAF routines. The object was not resolved, and had a flux ($i_{MDM} = 18.5$) in good agreement with the SDSS measurement (based on flux calibration using SDSS stars in the field). Further high-resolution observations are required to determine if this object has sub-arcsecond image splitting due to gravitational lensing. It is detected in 2MASS, with $J = 17.3 \pm 0.2$, $H = 16.3 \pm 0.2$, and $K = 15.9 \pm 0.2$.

5. DISCUSSION

One of our goals is to explore the properties of quasars not selected by SDSS. In this section we compile all available spectroscopic identifications of our candidates, and use this spectroscopic sample to explore the completeness of the SDSS.

It should be noted that our sample is drawn from the same imaging data as the SDSS quasar survey, and thus inherits many of the same limitations as that survey. For example, objects could be missed due to blending issues, lensed quasars could be misclassified as galaxies, and highly-extincted sources could fall below the flux limit even if their intrinsic luminosity is high. Our discussion of completeness is thus restricted to stellar objects detected above a given optical flux in the SDSS survey.

As described in the following section, roughly half of the objects in our sample have spectroscopic identifications. The spectroscopic sampling is derived from several sources, including color selection from the SDSS and radio selection from several surveys (including our own). While this sampling is not complete, it is sufficiently high such that we do not expect the population of unidentified objects to differ significantly from those that have been identified; we will justify this assumption for $z > 3.5$ quasars in §6.4.

5.1. Spectroscopic identifications of candidates

The complete set of quasar candidates identified by the selection described in § 3 includes 1536 objects to a

TABLE 3
FIRST/SDSS DR6 QUASARS
WITH $z > 3.5$

Name	z
SDSSJ084223.8+205543.3	3.57
SDSSJ085111.6+142337.8	4.21
SDSSJ094533.5+261115.6	3.58
SDSSJ102623.6+254259.6	5.28
SDSSJ103240.5+232820.6	3.53
SDSSJ103418.7+203300.2	5.00
SDSSJ121134.4+322615.2	4.11
SDSSJ130906.7+315800.2	3.93
SDSSJ131814.0+341805.6	4.82
SDSSJ135135.7+284014.8	4.73
SDSSJ135316.8+095636.7	3.62
SDSSJ135841.1+274708.1	3.93
SDSSJ141657.7+112247.6	3.89
SDSSJ142048.0+120546.0	4.03

TABLE 4
SPECTROSCOPIC IDENTIFICATIONS OF
CANDIDATES

Sample	N	QSOs	$z > 3.5$ QSOs
all	1536		
DR5QSO	385	385	93
DR6	219	79	14
NED	72	27	8
C08	18	18	16
MDM	45	29	7
total spec	739	538	138

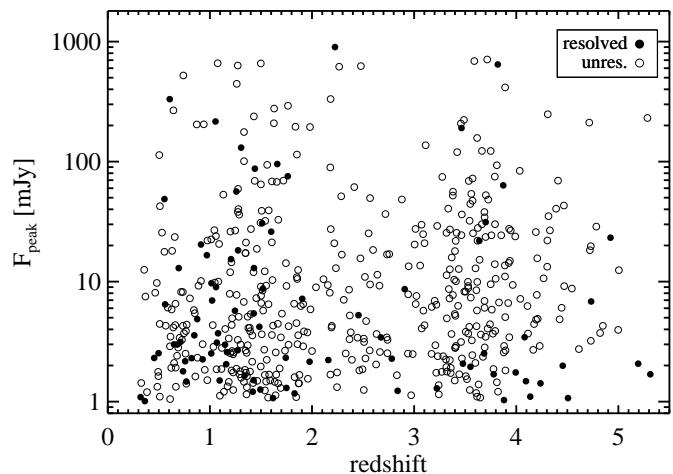


FIG. 4.— Peak radio flux density at 20cm vs. redshift for quasars in the sample. The distinction between resolved and unresolved radio sources is defined in §6.3.

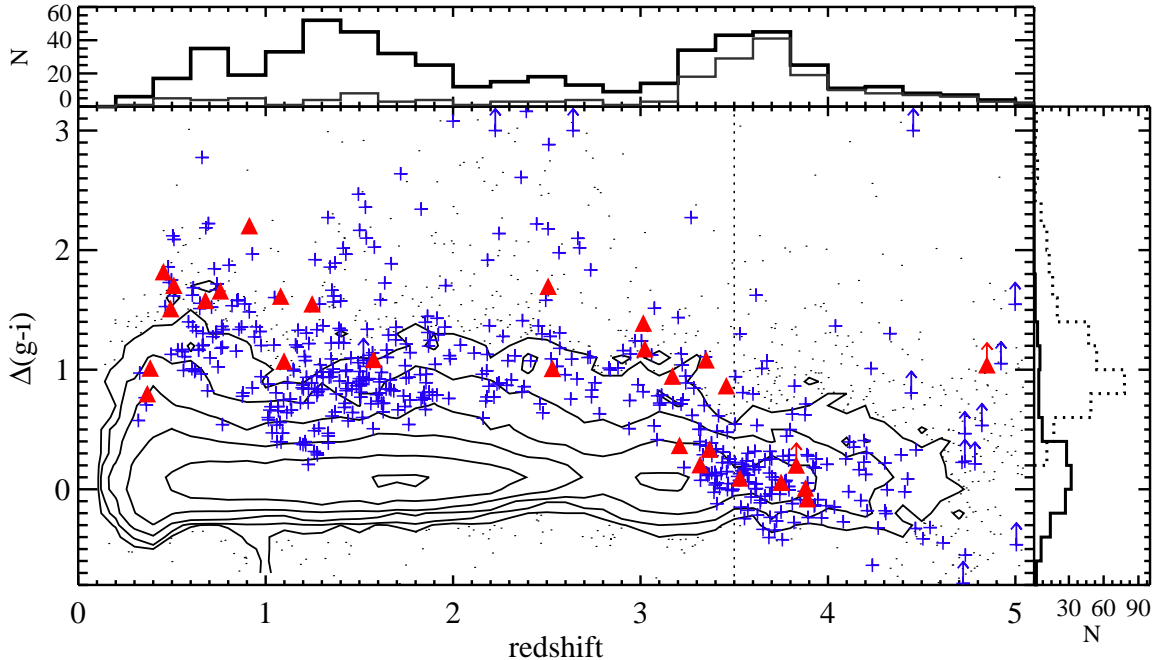


FIG. 5.— Relative colors of quasars (see definition in text). Shown as background contours and dots are DR5QSO, which peak at $\Delta(g-i) = 0$ at all redshifts (by definition). The contours begin when a cell (of size 0.1 along each axis) contains 5 objects, and each contour level represents an increase by a factor of 3 in number from the previous level. Blue crosses are spectroscopically confirmed quasars drawn from the radio-selected candidates presented here, and red triangles are quasars identified from MDM observations. The thick black line in the upper panel shows the redshift distribution of quasars in our radio-selected sample, and the thin gray line shows the subset of those quasars that were color-selected by SDSS. The panel on the right shows the distribution in relative color, with the thick solid line representing quasars with $z > 3.5$ and the dotted line representing quasars with $z < 3$. At $z < 3$, the radio-selected quasars are in the red tail of the color distribution, while at $z > 3.5$ they have similar colors to SDSS quasars.

flux limit of $i < 20.2$, covering 7900 deg^2 of the overlap between the FIRST and SDSS surveys. A total of 739 candidates have spectroscopic classifications, which we summarize here.

We begin by querying the SDSS DR6 SpecObj database for matches to our candidates, finding a total of 604 spectra. The most recent release of the SDSS quasar catalog is DR5QSO (Schneider et al. 2007), and contains quasars that have been confirmed by visual examination through the DR5 release. For spectra obtained prior to a modified Julian date of 53520 (roughly the cutoff of the DR5QSO catalog), we accept as quasars only those objects with matches in DR5QSO, resulting in 385 quasars and 109 objects rejected as quasars (including stars, galaxies, and unknown classifications). For the remaining spectra from DR6 (110 total), we visually examined the SDSS spectra and confirm 79 quasars. For the purposes of this work, we are most interested in high- z quasars, and thus in Table 3 we provide a list of 14 quasars from SDSS DR6 that we have verified to have $z > 3.5$. In total, SDSS provides 464 quasar identifications for our sample, with 107 at $z > 3.5$.

Next, we examine the NED database entries for each candidate. From this we find 27 additional quasars, many of which were radio-selected from previous surveys. The NED search adds 8 quasars at $z > 3.5$. We further include 18 quasar identifications from Carballo et al. (2008), including 16 at $z > 3.5$.

Last, we add our own spectroscopic sample, with 29 quasars at $z < 3.5$ and 7 at $z > 3.5$.

A summary of the sample is shown in Table 4. In total, of the 1536 candidates selected by the criteria outlined

in §3, 739 have spectroscopic identifications, and include 538 quasars and 138 $z > 3.5$ quasars. Figure 4 displays the radio fluxes of all quasars in the sample, showing that our selection method recovers radio quasars over a wide range of fluxes even at high redshifts.

5.2. Comparison to SDSS selection

Considering the candidate sample as a whole (1536 objects), about 1 in 5 are color-selected by SDSS. Since the results presented in Table 1 indicate that $\sim 70\%$ of the sample should consist of quasars based on a close radio source association, we now examine which quasars in our sample are missed by optical selection. We use relative colors to compare our sample to quasars from the SDSS. Relative color is defined as the difference between the color of an individual quasar and the modal color of quasars at the same redshift (Richards et al. 2001; Hopkins et al. 2004):

$$\Delta(g-i) = (g-i)_{\text{QSO}} - \langle (g-i) \rangle_z .$$

The modal colors for quasars as a function of redshift were obtained from Schneider et al. (2007). Figure 5 shows the $\Delta(g-i)$ color for our radio-selected sample compared to DR5QSO. At $z \gtrsim 3.5$, our criteria select quasars with colors similar to the SDSS sample. At lower redshifts, our candidates are much redder than average.

5.2.1. Reddened quasars at $z < 3$

Our red ugr color criteria select a large number of low-redshift quasars that are much redder than SDSS quasars. Of the 331 quasars with $z < 3$ in our sample, 254 (77%) have colors $\Delta(g-i) > 0.8$. By comparison,

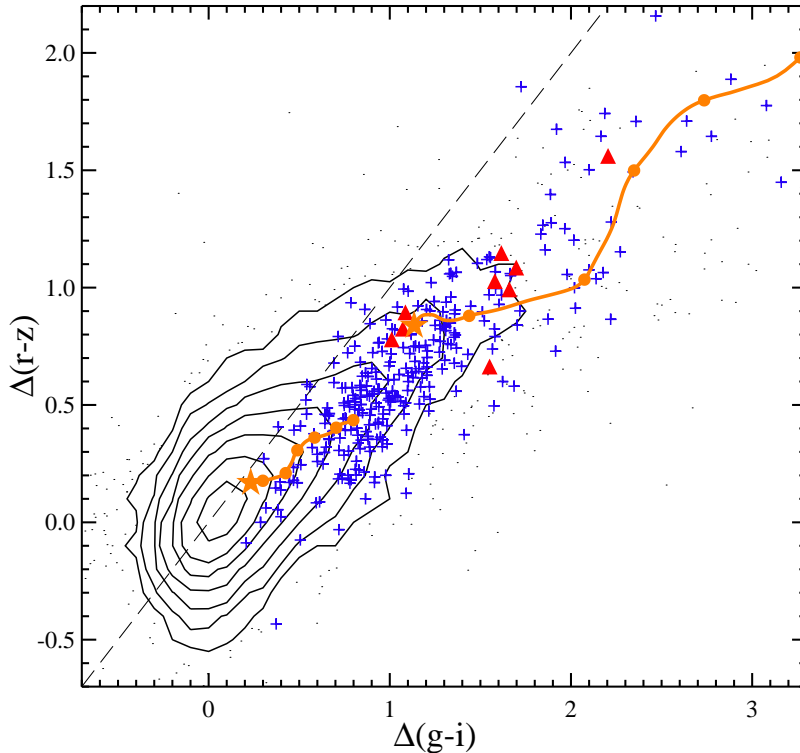


FIG. 6.— Relative colors showing curvature in the optical spectrum, for quasars with $0.6 < z < 3.0$. Contours and symbols are as in Figure 5. Quasars with power-law optical spectra should have $\Delta(g-i) \approx \Delta(r-z)$, shown by the dashed line (an object with an increasingly steep optical SED would move upward along the line). Most of the quasars have $\Delta(g-i) > \Delta(r-z)$, suggesting a curvature in the spectrum consistent with dust extinction. Two tracks show colors derived from a model quasar reddened by dust with $E(B-V) = 0.1$ (lower line) and $E(B-V) = 0.5$ (upper line). The beginning of the track at $z = 0.6$ is shown by a star, and filled circles show subsequent steps of $\Delta z = 0.4$.

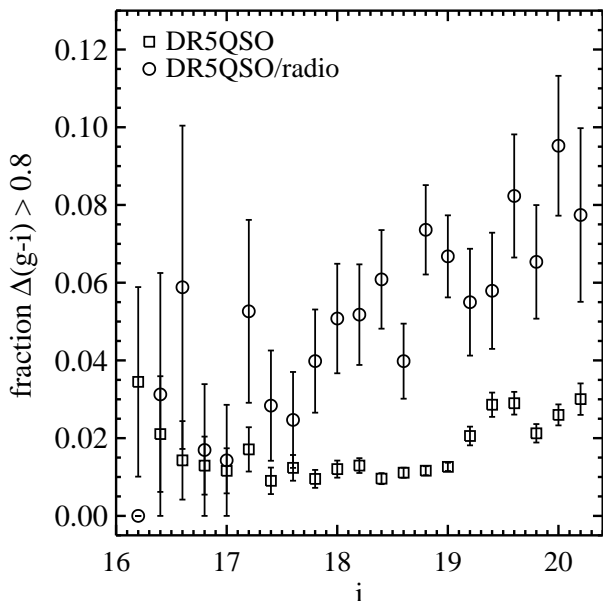


FIG. 7.— Fraction of SDSS quasars from DR5QSO with red colors, $\Delta(g-i) > 0.8$. Only quasars more luminous than $M_i < -23.5$ are included. The fraction is computed in bins of i magnitude and is given for all quasars (squares), and for only those with FIRST detections (circles). At $i > 19$, quasars are selected exclusively from $griz$ color space (QSO_HIZ), and the red fraction shows a significant jump. Across all magnitudes a larger fraction of FIRST-detected quasars are red, and the fraction increases steadily at fainter fluxes.

only 2% of DR5QSO are that red. Thus our selection criteria, which are designed for quasars at $z > 3.5$, also recover the red tail of lower redshift quasars.

These red, low-redshift quasars are unlikely to be color-selected by SDSS: only 16% of the radio-selected quasars with $\Delta(g-i) > 0.8$ and $z < 3$ meet the color selection criteria of SDSS. The low fraction of radio-selected quasars that were also optically-selected shows that SDSS color selection is not effective at identifying moderately-reddened quasars. This is because reddening removes quasars from $ugri$ selection, which is effective at $z \lesssim 2$ (our sample was selected to have little or no u -band flux). In addition, low-redshift quasars are not generally outliers from the stellar locus in $griz$ space, and reddening tends to push the colors along the locus.

Red quasars are necessarily found at faint optical magnitudes, eventually dropping out of optical surveys if the reddening is severe enough. Figure 7 shows the fraction of quasars from DR5QSO with colors redder than $\Delta(g-i) > 0.8$ as a function of observed flux. Only quasars more luminous than $M_i < -23.5$ (uncorrected for absorption) are included in the sample in order to eliminate contaminating light from the host galaxy. The fraction of red quasars increases at fainter fluxes, from $\sim 1.5\%$ at $i < 19$ to $\sim 3\%$ at $i > 19$. If only objects with FIRST counterparts are considered, the red fraction is higher across all fluxes, and is nearly 10% at the SDSS survey limit. It is notable that the red fraction among FIRST-detected sources with $i > 19.1$ is high even though this is below the limit of QSO-FIRST selection in SDSS. The high fraction of red sources among

quasars with FIRST detections implies a relationship between radio emission and optical color.

Radio surveys have been successful at discovering red quasars missed by optical surveys (Webster et al. 1995; White et al. 2003). However, it has been debated whether the radio-selected red quasars are indicative of a much larger (radio-faint) population missed by optical surveys, or rather that quasars with luminous radio emission are intrinsically redder on average. White et al. (2007) found that the median radio loudness in stacked radio images of SDSS quasars increases with redder optical colors (see their Figure 13). This result held even when only the radio emission from optically-selected quasars was included in the stack, eliminating any bias from objects selected on the basis of radio detection. Their findings strongly suggest that an intrinsic relationship exists between radio emission and optical color. Interestingly, the stack for the reddest sample they examined (roughly equivalent to $\Delta(g-i) = 0.8$) had a median radio flux density of 0.4 mJy, near the FIRST detection limit. This suggests that the reddest quasars should have a high likelihood of detection by FIRST, consistent with the results presented here.

Several studies have investigated whether the red colors seen in SDSS quasars arise from dust extinction or from an intrinsically red power-law continuum (Richards et al. 2003; Hopkins et al. 2004; Hall et al. 2006; Young et al. 2008). Dust extinction introduces curvature into the optical spectrum, whereas an intrinsically red continuum would show similar redness in all optical colors. Figure 6 shows the relative $\Delta(g-i)$ and $\Delta(r-z)$ colors for $z < 3$ quasars in our sample compared to DR5QSO. A dust-extincted quasar should have $\Delta(g-i) > \Delta(r-z)$, due to the curvature induced by the shape of the dust absorption spectrum (Hopkins et al. 2004; Hall et al. 2006). Essentially all of our red quasars have colors consistent with a dust-extincted spectrum. Figure 6 shows the effect of dust reddening on quasar colors using an SMC-type extinction law (Prevot et al. 1984; Pei 1992) with $E(B-V) = 0.1$ and $E(B-V) = 0.5$. The two tracks show the change in colors from $z = 0.6$ to $z = 3.0$ using the QSO spectral template from Vanden Berk et al. (2001). The quasars with $\Delta(g-i) > 0.8$ clearly follow the trend expected for dust reddening with $0.1 \lesssim E(B-V) \lesssim 0.5$. Previous surveys which combined FIRST with infrared data from 2MASS to identify highly-reddened quasars (Gregg et al. 2002; Glikman et al. 2004, 2007; Urrutia et al. 2008) typically find larger values of $E(B-V)$. This population can be considered to be only moderately reddened by comparison, and perhaps represents the continued evolution from heavily dust-obscured, Type 2 quasars to the unobscured, Type 1 population with blue optical colors.

5.2.2. Quasars at $z > 3.5$

At high redshift our criteria select quasars with similar colors to those from SDSS. Figure 5 shows that most of the radio-selected sample with $z > 3.5$ has $\Delta(g-i) \sim 0$. At $z > 3.5$ the QSO_HIZ algorithm is very effective; only a handful of quasars identified by other means (usually radio selection) are missed by the algorithm. Of the 138 quasars in our sample with $z > 3.5$, 111 are QSO_HIZ targets, suggesting that the color selection of SDSS is 80% complete in this redshift range. When QSO_FIRST

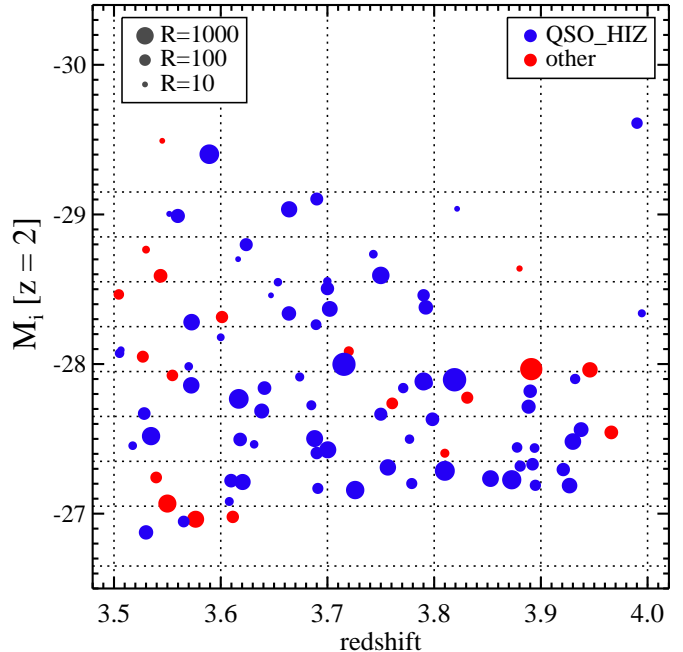


FIG. 8.— Redshift/luminosity distribution of FIRST/SDSS quasars at $3.5 < z < 4.0$. The symbol size is proportional to the radio loudness. Blue circles denote quasars with the QSO_HIZ flag, and red circles denote quasars without the QSO_HIZ flag.

TABLE 5
REDSHIFT COMPLETENESS OF SDSS

z_1	z_2	N_{QSO}	QSO_HIZ ^a	primary ^b
3.50	3.60	22	13 (0.59)	18 (0.82)
3.60	3.70	26	24 (0.92)	25 (0.96)
3.70	3.80	19	17 (0.89)	18 (0.95)
3.80	3.90	16	12 (0.75)	12 (0.75)
3.90	4.00	9	7 (0.78)	7 (0.78)
3.50	4.00	92	73 (0.79)	80 (0.87)

^a QSO_HIZ targets in SDSS.

^b Primary quasar targets in SDSS.

selection is included, the SDSS primary target criteria for quasars select 118 of the $z > 3.5$ sample (86%). This is in good agreement with the $\sim 85\%$ completeness for SDSS in this redshift range derived by R06.

As noted in §4, the MDM sample was drawn uniformly from the set of previously unidentified candidates, other than a preference for objects with $i \sim 19.5$. Of the seven $z > 3.5$ quasars identified by MDM observations, one had the QSO_FIRST flag, two had the QSO_HIZ flag, and J0741+2520 (at $z = 5.2$) had both flags. These four objects were primary quasar targets in SDSS but did not have spectra obtained in the main survey. One object, at $z = 3.88$, was bright enough for QSO_FIRST selection ($i = 18.7$) but had the BLENDED flag set and thus was rejected by the SDSS quasar targeting pipeline. The remaining two, at $z = 3.83$ and $z = 4.85$, were too faint for QSO_FIRST selection and were not color-selected. Thus only three of the 45 candidates observed at MDM were $z > 3.5$ quasars missed by SDSS quasar selection.

Figure 8 shows the distribution of our radio-selected quasar sample in the redshift-optical luminosity plane. We derive the absolute magnitude $M_i(z = 2)$ using the k -corrections provided in R06; this is the absolute i -band magnitude for the object if it were at $z = 2$. It is clear from this figure that while SDSS color selection is effective in the redshift range we consider (few radio quasars are missed overall), it is much lower at $z \sim 3.5$ than at higher redshifts. Table 5 shows the completeness of SDSS as a function of redshift, measured against our radio-selected sample. QSO_HIZ selection is 80-90% effective at $3.6 < z < 4.0$, but only $\sim 60\%$ effective at $3.5 < z < 3.6$. This is consistent with the results presented by R06; their Figure 10 shows that the SDSS selection function experiences a local minimum near $z \sim 3.5$.

There is a noticeable lack of points in the upper right part of Figure 8, as there appears to be a significant drop in the number of highly-luminous quasars with increasing redshift. Some decrease is to be expected, owing to the steep decline in comoving quasar number density with redshift at $z > 3$. However, the best-fit luminosity function of R06 predicts a factor of ~ 2 fewer quasars with $M_i < -28.3$ at $z = 4$ compared to $z = 3.5$, whereas the number of luminous radio-selected quasars in our sample drops by a factor of ~ 4 over the same redshift interval. These quasars are bright enough for QSO_FIRST selection, and should be well-sampled by the SDSS. We estimate the number of luminous quasars detectable by FIRST over this redshift interval by scaling the R06 optical luminosity function by 10% and find reasonable agreement given the limited sample size. Thus while the drop in highly-luminous quasars with redshift is suggestive, the numbers in this study are too small to interpret it further.

6. LUMINOSITY FUNCTION OF $3.5 < Z < 4.0$ RADIO-LOUD QUASARS

In the preceding section we established that our sample of high-redshift quasars is similar to those found by the SDSS. We now use our sample to construct a luminosity function for radio-loud quasars, and compare it to the SDSS results for optically-selected quasars. We consider only quasars with $3.5 < z < 4.0$, as our survey was designed to be highly efficient in this redshift range. At higher redshifts the number of sources is too small to allow meaningful results.

Because we are combining selection from optical and radio surveys with different depths, we define our limiting depth by the ratio of radio and optical flux. Thus we are deriving a luminosity function for quasars which, at a given optical luminosity, have a radio loudness R^* greater than a specified value. We define radio loudness as $R^* = S_{5\text{GHz}}/S_{2500}$, in terms of the rest-frame flux densities at 5 GHz and 2500Å (e.g., Stocke et al. 1992). As the radio and optical fluxes are generally assumed to have the same power-law slope ($\alpha_{rad} = \alpha_{opt} = -0.5$), and emission line effects are small over the redshift range under consideration, no formal k -correction is necessary when calculating the ratio; however, we do make a slight correction using the assumed slope to bring the observed 1.4 GHz and i -band fluxes to rest-frame 5 GHz and 2500Å. We adopt a limit of $R^* = 70$, which for a quasar with $i = 20.2$ at $z = 4$ corresponds to a 20cm flux density of $\sim 2\text{mJy}$. Adopting a somewhat high limit in R^*

alleviates the incompleteness to the detection of faint radio sources described below, but means that we are not including all radio-loud quasars according to the usual threshold of $R^* > 10$.

Before constructing a luminosity function from our sample, we must first account for several sources of incompleteness.

6.1. Optical detection

At the faint limit of our sample, $i = 20.2$, SDSS is highly complete. In constructing the SDSS QSO luminosity function, R06 applied a 5% correction to account for image quality incompleteness, which arises from objects missed due to fatal and non-fatal photometric errors. The SDSS quasar survey rejects objects with the fatal error BLENDED, whereas we include such objects. By examining roughly two million randomly-selected stars from the SDSS with $18.5 < i < 20.2$, we find that $\sim 5\%$ have the BLENDED flag, while $\sim 1\%$ have other fatal photometric errors. These fractions agree well with the occurrence of these errors in our sample (see § 3). Of the 76 BLENDED objects in our sample, 17 have spectroscopic identifications, 10 of which (59%) are quasars, including 2 (12%) at $z > 3.5$. Thus the fraction of quasars among BLENDED objects is similar to the sample as a whole. We apply a 1% correction to account for the remaining photometric errors.

6.2. Radio detection

The nominal detection limit of the FIRST survey is 1mJy. However, the completeness at faint fluxes is different for point and extended sources, and thus the average completeness for a population depends on its angular size distribution. This completeness has been calculated specifically for SDSS quasars, and is given in Figure 1 of Jiang et al. (2007). We impose a limit of $S_{1.4} > 2\text{mJy}$ for our sample; FIRST is $\gtrsim 85\%$ complete at this limit. We use the curve given in Figure 1 of Jiang et al. (2007) to correct for incompleteness to faint radio sources using the integrated FIRST flux; in general this correction is small.

6.3. Optical/Radio offset

Our choice of a tight matching radius between the optical and radio positions greatly improves the efficiency of our survey at the expense of completeness. In order to measure this completeness, we identify FIRST counterparts to quasars from DR5QSO using the method of Lu et al. (2007), which accounts for extended and multi-component radio source counterparts to optical quasars. We consider any FIRST source within $2''$ of the optical position as a “core” radio counterpart, and allow for “coreless” FR II-type radio counterparts by identifying pairs of radio sources located symmetrically about the optical position with an opening angle $> 150^\circ$ and a total separation $< 2'$ (see Lu et al. 2007; de Vries et al. 2006). In total, we find that $\sim 9\%$ of DR5QSO have FIRST counterparts, and $\sim 5\%$ of those do not have a core within $2''$.

We then compute the fraction of FIRST counterparts to quasars from DR5QSO that are within $0.5''$ of the optical position. Figure 9 shows this distribution as a function of the FIRST flux density. We further divide

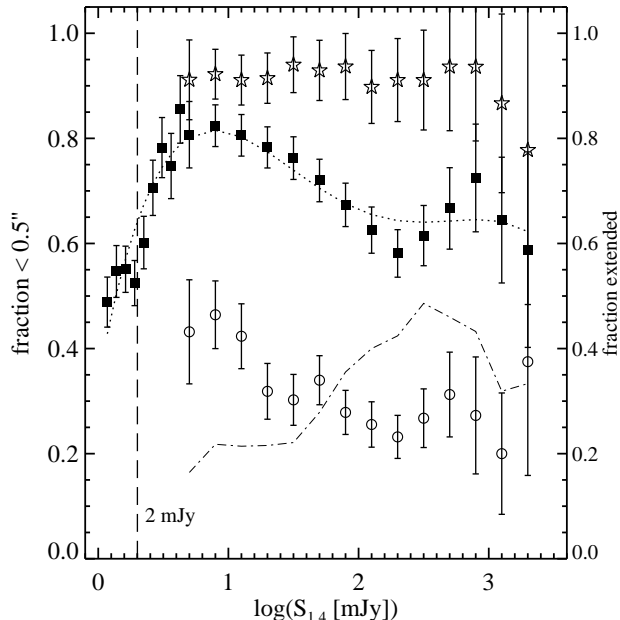


FIG. 9.— Fraction of FIRST matches to DR5QSO that are within $0.5''$. Extended (resolved) FIRST counterparts are shown as circles, compact (unresolved) counterparts are shown as stars. The combined distribution is shown as filled squares, along with a fourth-order polynomial function fit to this distribution (dotted line). The fraction of extended counterparts as a function of 1.4 GHz flux density is shown as a dot-dashed line. At faint fluxes ($S_{1.4} \lesssim 5$ mJy) the distinction between compact and extended counterparts breaks down, and thus we only show the combined distribution.

the sample into extended and compact radio sources, by defining a dimensionless concentration parameter $\theta = (F_{int}/F_{peak})^{1/2}$ (Ivezić et al. 2002), which is the geometric mean of the major and minor axis lengths. The concentration is calculated using the peak and integrated flux densities from the FIRST catalog, as measured for the core radio counterpart. Following Kimball & Ivezić (2008), we classify radio sources with a concentration $\theta > 1.06$ as extended and those with $\theta \leq 1.06$ as compact. All coreless radio counterparts are classified as extended.

Over 90% of quasars in DR5QSO with compact radio counterparts brighter than 5 mJy have optical-radio offsets less than $0.5''$. However, at faint radio fluxes, the FIRST astrometric uncertainties increase and a greater number of sources are missed. In addition, the centroid of extended radio sources may not be well-aligned with the optical position, and thus across all radio fluxes we miss a greater number of extended radio sources. About 20-30% of FIRST counterparts to SDSS quasars are extended, and even for bright extended sources we only recover $\sim 25 - 30\%$ with a $0.5''$ matching radius. Overall, we find the completeness for a $0.5''$ matching radius to be $\sim 74\%$ for sources with $F_{int} > 2$ mJy, which is in good agreement with a similar calculation by Lu et al. (2007, their Figure 5).

Figure 9 shows a fourth-order polynomial fit to the matching completeness, which accounts for the dependence on radio source flux and morphology while smoothing the distribution. We use this polynomial fit to weight quasars in our sample by their radio flux in order to account for objects missed by matching the optical and

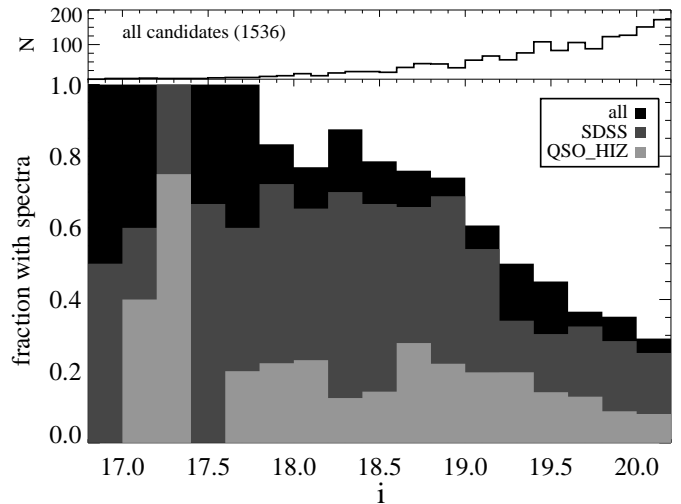


FIG. 10.— Spectroscopic coverage of the candidates, expressed as the fraction of candidates per magnitude bin ($\Delta m = 0.2$) that have spectroscopic identifications. Most of the spectra come from SDSS, but at $i > 19$ the coverage drops considerably, as the candidates are too faint for QSO-FIRST selection, and only a small percentage are color-selected (QSO_HIZ). Among the candidates with spectra, the fraction of $z > 3.5$ quasars is roughly constant with i magnitude, at $\sim 17\%$.

radio data.

6.4. Spectroscopic coverage

Fewer than half of our photometric candidates have been observed spectroscopically. Figure 10 shows the spectroscopic coverage of the full candidate sample of 1536 objects. At $i < 19$, about 80% of the candidates have spectroscopic identifications, while at fainter magnitudes the coverage drops, falling as low as $\sim 30\%$ at $i = 20.2$. Most of the spectroscopic identifications come from the SDSS, though a majority of those were either selected by QSO-FIRST or serendipity criteria.

In order to correct for the lack of complete spectroscopic coverage for our candidates, we must account for the fact that the objects which do have spectra were not chosen uniformly. Objects that are primary quasar targets in SDSS are the most likely to have spectral identifications; over 81% of the 524 primary targets have identifications. This fraction is independent of optical magnitude, and reflects the rate at which primary quasar targets were assigned spectroscopic fibers during the course of the survey. In §5.2.2 we showed that QSO_HIZ selection is highly effective for $z > 3.5$ quasars with $i < 20.2$. As this selection misses few quasars, a greater fraction of objects with the QSO_HIZ flag are expected to be high-redshift quasars, as compared to the (much larger) population of objects without that flag. Half of the 217 QSO_HIZ objects among our candidates with spectroscopic identifications are $z > 3.5$ quasars. On the other hand, only 5% of the 520 candidates that have identifications and are not QSO_HIZ are $z > 3.5$ quasars. This shows that the spectroscopic coverage of high- z quasars in our sample is high, and we do not expect a significant number of such objects to be left among the objects without spectroscopy.

Quasars that are SDSS primary targets are given a weight of $1/0.81$ to account for the spectroscopic in-

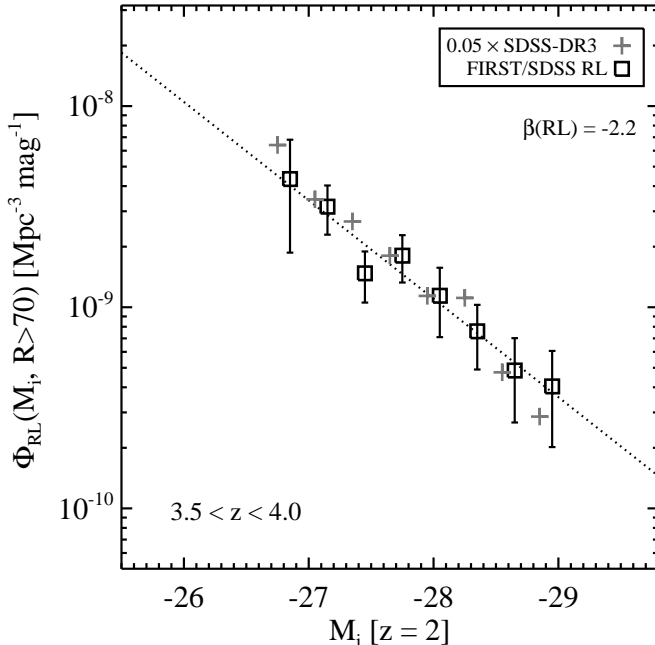


FIG. 11.— Luminosity function of $3.5 < z < 4.0$ radio-loud quasars with $R^* > 70$, shown as squares with Poisson error bars. For comparison, gray crosses show the luminosity function calculated from SDSS over this redshift interval by R06, scaled by a factor of 0.05 (see Table 6 of R06). The dotted line shows the best-fit slope, $\beta_{\text{RL}} = 2.2$.

completeness of the SDSS. For objects that are not primary targets, the fraction that have been observed spectroscopically is strongly dependent on optical flux. We find that the fraction of non-primary targets with spectra can be described by the linear relation $f_{\text{spec}} = 0.8 - 0.2 \times (i - 17.0)$ (see Figure 10), and thus non-primary objects are weighted by the inverse of this function. Applying a weight in this fashion assumes that the non-primary targets with spectroscopic identifications were selected uniformly. We consider this to be a fair assumption as these objects were either serendipitous targets in SDSS, or found in radio surveys such as ours that employed broad color criteria.

This weighting is based on the optical flux distribution of the quasars, and not their luminosities. An alternative method for determining the completeness is to assume an *a priori* distribution in color and absolute magnitude as a function of redshift and then compare to the observed distribution, as was done by R06. We are instead assuming that the candidates with spectra are a fair sample of the remaining unidentified candidates and that our completeness in terms of optical color is high, such that we can estimate the spectroscopic incompleteness simply in terms of the probability that a given candidate has been observed spectroscopically.

6.5. Luminosity Function

Having corrected our sample for all the sources of incompleteness listed above, we now use the sample to calculate a luminosity function for radio-loud quasars at $3.5 < z < 4.0$. We derive this function in terms of the optical luminosity in order to compare with results from SDSS. As our sample is limited to luminous quasars

TABLE 6
RADIO-LOUD QLF AT $3.5 < z < 4.0$

M_i	N	N_{RL}	$N_{\text{RL}}^{\text{corr}}$	Φ_{RL}	$\Phi_{\text{RL}}/\Phi_{\text{SDSS}}$
(1)	(2)	(3)	(4)	(5)	(6)
-28.95	7	4	7.1	0.404	7.02
-28.65	13	5	8.5	0.485	5.07
-28.35	13	8	13.3	0.759	3.39
-28.05	16	8	20.0	1.141	4.98
-27.75	21	16	31.6	1.804	4.97
-27.45	20	14	25.8	1.474	2.74
-27.15	19	18	45.2	3.162	4.57
-26.85	4	4	14.4	4.337	3.37

NOTE. — Columns are (1) M_i , (2) the number of FIRST/SDSS quasars in the bin, (3) the number of radio-loud quasars in the bin ($R > 70$), (4) the corrected number of radio-loud quasars in the bin after applying the incompleteness weights, (5) RLQLF in units of 10^{-9} Mpc $^{-3}$ mag $^{-1}$, (6) ratio of RLQLF to SDSS QLF, multiplied by 100.

($M_i \lesssim -27$), we model the luminosity function as a single power law, $\Phi_{\text{RL}} \propto L^{\beta_{\text{RL}}}$, where RL denotes that we are considering only radio-loud quasars. We construct a binned radio-loud quasar luminosity function (RLQLF) according to the prescription of Page & Carrera (2000), using the $1/V_{\text{max}}$ method (Schmidt 1968; Avni & Bahcall 1980) in discrete magnitude bins. Table 6 and Figure 11 show the resulting RLQLF for radio-loud quasars with $R > 70$, and also compare the values we have derived for radio-loud quasars to those calculated by R06 for quasars from the SDSS.

Overall, there is good agreement between the two luminosity functions, after scaling the optical luminosity function by 5%. The best-fit slope is slightly flatter, with $\beta_{\text{RL}} = -2.2 \pm 0.2$, compared to $\beta \sim -2.4$ as derived by R06 from SDSS data (see their Figure 21). The agreement between the shapes of the luminosity functions provides some corroboration for the assertion that the bright-end slope of the QLF flattens at high redshift (compared to $\beta \approx -3$ at $z \lesssim 2$).

It has been suggested that the fraction of radio-loud quasars (with $R^* > 10$) declines with both redshift and optical luminosity (Jiang et al. 2007). Such an effect might account for the relatively low radio-loud fraction of $\sim 5\%$ derived by comparing the space densities of radio-loud quasars to the optical population (Table 6), as well as the somewhat flatter slope – a decline of the radio-loud fraction with optical luminosity would tend to flatten the RLQLF. However, we note that our sample is restricted to radio-loud quasars with $R^* > 70$ and thus underrepresents the radio-loud fraction according to the threshold usually adopted, which would include objects with $10 < R^* \leq 70$. Further, Jiang et al. (2007) found that the radio-loud fraction depends on optical luminosity as $\sim L^{0.5}$, implying that $\beta_{\text{RL}} \sim \beta_{\text{SDSS}} + 0.5$, which is a greater difference between the two slopes than we find. A larger sample of high- z quasars with radio coverage deeper than that of FIRST is needed to better address this question.

7. CONCLUSIONS

We have assembled a sample of $z > 3.5$ radio quasar candidates using a simple color cut, and shown that precise matching of the radio and optical positions leads to a high rate of discovery. We have identified 29 quasars, 26 of which are published for the first time, with 7 at $z > 3.5$ and the highest redshift source at $z = 5.2$.

The SDSS does an excellent job of identifying quasars at a wide range of redshifts, and $\sim 85\%$ of $z > 3.5$ quasars in our radio-selected quasar sample were targeted by the color selection algorithms of SDSS. However, it achieves a high degree of completeness at the expense of efficiency, with the primary algorithm used to target high- z quasars having a 50% stellar contamination rate.

We have shown that radio selection, when optimized to the astrometric precisions of the parent surveys and combined with simple, relatively unbiased color selection, can identify high-redshift quasars with high efficiency. Our particular criteria were used to target quasars at $z > 3.5$ and are 20% efficient at those redshifts. Applying red color selection criteria yields two types of objects: low-redshift, moderately reddened quasars largely missed by optical selection, and high-redshift quasars similar to those found in optical surveys. We used our radio-selected sample of $z > 3.5$ quasars to derive a completeness for SDSS selection at high redshift, and found the completeness to be high ($\sim 85\%$) and in good agreement with previous results. We further use the sample to derive a radio-loud quasar luminosity function at $3.5 < z < 4.0$, and again find good agreement with SDSS results.

More sophisticated quasar selection methods, such as the automated neural networks employed by Carballo et al. (2008), can achieve even higher efficiencies ($\sim 70\%$). This potentially comes at the expense of completeness, and the selection function can be difficult to quantify. In addition, these methods require a training set of known objects, meaning that the candidates identified by the algorithm will generally have similar properties to the input objects, and are subject to any limitations inherent to that sample. Broad criteria such as ours are much less efficient, but better suited for constructing complete samples.

We have employed radio selection in order to expand on color selection techniques. Currently planned synoptic surveys such as PAN-STARRS and LSST will be able to distinguish quasars from stars through optical variability and (lack of) proper motion, and thus find quasars independent of their optical colors. The LSST design will allow detection of quasars to the formal luminosity cutoff ($M < -23$) to $z \sim 5$ without using color selection (Ivezić et al. 2008). Moderately reddened quasars

similar to those presented here will fall within reach of this survey. However, for some heavily-extincted quasars the nucleus may be sufficiently obscured such that any variability would pass unnoticed, or worse, the observed flux would fall below the survey detection limit. These quasars can be found through infrared-excess selection (IRX, Warren et al. 2000), which is relatively insensitive to reddening, using a new generation of infrared surveys much deeper than 2MASS (e.g., UKIDSS, VIKING, VHS; for an example with UKIDSS see Maddox et al. 2008). These surveys will better address the connection between radio luminosity and optical color by having sensitivity to red quasars without requiring radio detection for selection. Finally, FIRST only detects the most radio-loud quasars at high-redshift; future surveys with the greatly enhanced sensitivity of the EVLA will push deeper into the radio-loud quasar luminosity function at high- z .

8. ACKNOWLEDGEMENTS

We thank Zoltán Haiman and Željko Ivezić for suggestions which improved the paper, and Jules Halpern for assistance with the MDM spectroscopy. We also thank the anonymous referee for suggestions which improved the manuscript.

Funding for the SDSS and SDSS-II has been provided by the Alfred P. Sloan Foundation, the Participating Institutions, the National Science Foundation, the U.S. Department of Energy, the National Aeronautics and Space Administration, the Japanese Monbukagakusho, the Max Planck Society, and the Higher Education Funding Council for England. The SDSS Web Site is <http://www.sdss.org/>.

The SDSS is managed by the Astrophysical Research Consortium for the Participating Institutions. The Participating Institutions are the American Museum of Natural History, Astrophysical Institute Potsdam, University of Basel, University of Cambridge, Case Western Reserve University, University of Chicago, Drexel University, Fermilab, the Institute for Advanced Study, the Japan Participation Group, Johns Hopkins University, the Joint Institute for Nuclear Astrophysics, the Kavli Institute for Particle Astrophysics and Cosmology, the Korean Scientist Group, the Chinese Academy of Sciences (LAMOST), Los Alamos National Laboratory, the Max-Planck-Institute for Astronomy (MPIA), the Max-Planck-Institute for Astrophysics (MPA), New Mexico State University, Ohio State University, University of Pittsburgh, University of Portsmouth, Princeton University, the United States Naval Observatory, and the University of Washington.

Facilities: Hiltner (CCDS,Retromcam)

REFERENCES

- Avni, Y., & Bahcall, J. N. 1980, ApJ, 235, 694
 Becker, R. H., White, R. L., & Helfand, D. J. 1995, ApJ, 450, 5
 Benn, C. R., Vigotti, M., Pedani, M., Holt, J., Mack, K.-H., Curran, R., & Sánchez, S. F. 2002, MNRAS, 329, 221
 Carballo, R., González-Serrano, J. I., Benn, C. R., & Jiménez-Luján, F. 2008, MNRAS, 391, 369
 Carballo, R., González-Serrano, J. I., Montenegro-Montes, F. M., Benn, C. R., Mack, K.-H., Pedani, M., & Vigotti, M. 2006, MNRAS, 370, 1034
 de Vries, W. H., Becker, R. H., & White, R. L. 2006, AJ, 131, 666
 Fan, X., et al. 2001, AJ, 121, 54
 Ferrarese, L., & Merritt, D. 2000, ApJ, 539, L9
 Glikman, E., Gregg, M. D., Lacy, M., Helfand, D. J., Becker, R. H., & White, R. L. 2004, ApJ, 607, 60
 Glikman, E., Helfand, D. J., White, R. L., Becker, R. H., Gregg, M. D., & Lacy, M. 2007, ApJ, 667, 673
 Gregg, M. D., Lacy, M., White, R. L., Glikman, E., Helfand, D., Becker, R. H., & Brotherton, M. S. 2002, ApJ, 564, 133
 Hall, P. B., et al. 2002, ApJS, 141, 267
 Hall, P. B., Gallagher, S. C., Richards, G. T., Alexander, D. M., Anderson, S. F., Bauer, F., Brandt, W. N., & Schneider, D. P. 2006, AJ, 132, 1977

- Holt, J., Benn, C. R., Vigotti, M., Pedani, M., Carballo, R., González-Serrano, J. I., Mack, K.-H., & García, B. 2004, *MNRAS*, 348, 857
- Hook, I. M., Becker, R. H., McMahon, R. G., & White, R. L. 1998, *MNRAS*, 297, 1115
- Hook, I. M., McMahon, R. G., Patnaik, A. R., Browne, I. W. A., Wilkinson, P. N., Irwin, M. J., & Hazard, C. 1995, *MNRAS*, 273, L63
- Hopkins, P. F., et al. 2004, *AJ*, 128, 1112
- Ivezić, Ž., et al. 2002, *AJ*, 124, 2364
- Ivezić, Z., et al. 2008, arXiv:0805.2366
- Jiang, L., Fan, X., Ivezić, Ž., Richards, G. T., Schneider, D. P., Strauss, M. A., & Kelly, B. C. 2007, *ApJ*, 656, 680
- Kimball, A. E., & Ivezić, Ž. 2008, *AJ*, 136, 684
- Kimball, A. E., Knapp, G. R., Ivezić, Z., West, A. A., Bochanski, J. J., Plotkin, R. M., & Gordon, M. S. 2009, arXiv:0906.3030
- Lu, Y., Wang, T., Zhou, H., & Wu, J. 2007, *AJ*, 133, 1615
- Maddox, N., Hewett, P. C., Warren, S. J., & Croom, S. M. 2008, *MNRAS*, 386, 1605
- McGreer, I. D., Becker, R. H., Helfand, D. J., & White, R. L. 2006, *ApJ*, 652, 157
- Morgan, C. W., Byard, P. L., DePoy, D. L., Derwent, M., Kochanek, C. S., Marshall, J. L., O'Brien, T. P., & Pogge, R. W. 2005, *AJ*, 129, 2504
- Page, M. J., & Carrera, F. J. 2000, *MNRAS*, 311, 433
- Pei, Y. C. 1992, *ApJ*, 395, 130
- Prevot, M. L., Lequeux, J., Prevot, L., Maurice, E., & Rocca-Volmerange, B. 1984, *A&A*, 132, 389
- Richards, G. T., et al. 2002, *AJ*, 123, 2945
- Richards, G. T., et al. 2001, *AJ*, 121, 2308
- Richards, G. T., et al. 2003, *AJ*, 126, 1131
- Richards, G. T., et al. 2006, *AJ*, 131, 2766
- Sandage, A. 1965, *ApJ*, 141, 1560
- Schmidt, M. 1963, *Nature*, 197, 1040
- Schmidt, M. 1968, *ApJ*, 151, 393
- Schmidt, M., Schneider, D. P., & Gunn, J. E. 1995, *AJ*, 110, 68
- Schneider, D. P., et al. 2007, *AJ*, 134, 102
- Snellen, I. A. G., McMahon, R. G., Dennett-Thorpe, J., Jackson, N., Mack, K.-H., & Xanthopoulos, E. 2001, *MNRAS*, 325, 1167
- Stocke, J. T., Morris, S. L., Weymann, R. J., & Foltz, C. B. 1992, *ApJ*, 396, 487
- Urrutia, T., Becker, R. H., White, R. L., Glikman, E., Lacy, M., Hodge, J., & Gregg, M. D. 2008, arXiv:0808.3668
- van Dokkum, P. G. 2001, *PASP*, 113, 1420
- Vanden Berk, D. E., et al. 2001, *AJ*, 122, 549
- Vanden Berk, D. E., et al. 2005, *AJ*, 129, 2047
- Warren, S. J., Hewett, P. C., & Foltz, C. B. 2000, *MNRAS*, 312, 827
- Webster, R. L., Francis, P. J., Peterson, B. A., Drinkwater, M. J., & Masci, F. J. 1995, *Nature*, 375, 469
- White, R. L., Helfand, D. J., Becker, R. H., Glikman, E., & de Vries, W. 2007, *ApJ*, 654, 99
- White, R. L., Helfand, D. J., Becker, R. H., Gregg, M. D., Postman, M., Lauer, T. R., & Oegerle, W. 2003, *AJ*, 126, 706
- York, D. G., et al. 2000, *AJ*, 120, 1579
- Young, M., Elvis, M., & Risaliti, G. 2008, *ApJ*, 688, 128